buildings

MDPI

Article

Angle Control Algorithm for Air Curtain Based on GA Optimized Quadratic BP Neural Network

Yuxi Zhao, Liguo Shuai *, Haodong Zhang and Yuhang Zheng

School of Mechanical Engineering, Southeast University, Nanjing 211189, China; 220230367@seu.edu.cn
* Correstpondence: 101008891@seu.edu.cn

Abstract: In air conditioning systems, air curtains play a crucial role in reducing the exchange of hot and cold air between the interior and exterior environments. Nevertheless, the majority of current air curtains suffer from limited airtightness and real-time performance due to their complex jet trajectory, relying on traditional control methods. Thus, this paper introduces an angle control algorithm for air curtains based on a GA-optimized quadratic BP neural network. Initially, the BP neural network is trained using the Hayes dataset to develop the prediction model for temperature-jet angle. Subsequently, the optimization model for jet angles-windshield angle is constructed, and the optimal angles set meeting the fitness function is identified using GA global search. Later, the prediction model and the optimal angles set are once again trained using the BP neural network to generate prediction model for temperature-jet angles and windshield angle. Following CFD simulation, the airtightness indicator demonstrated a 26.5% improvement with the proposed control method compared to traditional ones, highlighting the superior airtightness. In comparison to other algorithms, the proposed algorithm demonstrates a remarkable 89% enhancement in real-time performance and stronger robustness. This study presents a novel approach for the intelligent control of air curtains, holding significant importance in advancing the intelligent development of air curtain technology and facilitating energy efficiency and emission reduction.

Keywords: BP neural network; genetic algorithm; air curtain; control system; CFD simulation

check for updates

Citation: Zhao, Y.; Shuai, L.; Zhang, H.; Zheng, Y. Angle Control Algorithm for Air Curtain Based on GA Optimized Quadratic BP Neural Network. *Buildings* **2024**, *14*, 3144. https://doi.org/10.3390/buildings14103144

Academic Editor: Antonio Caggiano

Received: 11 August 2024
Revised: 27 September 2024
Accepted: 28 September 2024
Published: 2 October 2024

Copyright: © 2024 by the authors. Licensee MDPI, Basel, Switzerland. This article is an open access article distributed under the terms and conditions of the Creative Commons Attribution (CC BY) license (https://creativecommons.org/licenses/by/4.0/).

1. Introduction

The airconditioning equipment system produces greenhouse gas emissions due to direct or indirect energy consumption worldwide, which has deep impacts on global climate change. Frequent exchange of hot and cold air caused by long operation hours and constant entry and exit significantly increases the load on the air-conditioner. Based on statistics, the penetration of warm outside air through doorways accounts for more than half of the total cooling load [1]. Therefore, commonly used to address the requirement for balancing personnel access and temperature control, air curtains play a vital role in reducing energy consumption and carbon dioxide emissions by facilitating heat exchange [2]. Studies have shown that they can reduce energy consumption by up to 80% and carbon dioxide emissions by up to 60.5% [3]. Nevertheless, commercially available air curtains still rely on traditional control methods, which generate complex nonlinearities, time-varying uncertainties that are becoming increasingly prominent, and cause limitations in airtightness and realvtime performance. Thus, developing an intelligent control system with real-time optimization and control capabilities for air curtains holds paramount significance in advancing the intelligent evolution of air curtain technology and promoting energy conservation initiatives.

The performance of air curtain devices, in terms of blowing forms and other designs, has been the subject of relatively extensive and theoretical research by many researchers [4–6]. In 2000, Guyonnaud et al. [7] synthesized earlier findings and introduced an equation for air curtain dynamics, incorporating variables such as tunnel height, air curtain jet angle,

jet velocity, and turbulence intensity. Advances in computer technology have facilitated the development of more complex modeling and validation capabilities. Foster and his team [8,9] rectified the insufficient lateral modeling information in 2D models through the application of Computational Fluid Dynamics (CFD). Gonçalves et al. [10–12] applied the CFX module to determine air infiltration at varying jet velocities. Despite the ability of advanced transient models to accurately depict real-time losses under various factors, the emphasis on factor analysis and jet dynamics has limited practical application due to the complexity and inefficiency of simulations.

Recently, scholars worldwide have been conducting more research on the airtightness of air curtains. Ashika Rai [13–15] examined the influence of the jet angle and found that adjusting it to 10° outward, as opposed to 0°, resulted in better control due to natural convection, thereby achieving energy savings of 17.6%. Nevertheless, optimization strategies, including methods for adjusting and controlling the exhaust angle, have received limited attention and analysis. Sun Jining and his team [16] conducted a comprehensive study on the relationship between the performance of vertical multilevel refrigerated demonstration cabinets and various configurations of air-guiding strips. Japanese scholar Shih-Heng Lee [17] assessed the safety factor of deflection modulus for both non-circulating and circulating air curtains by correlating up-fed and side-fed air curtains and determined their optimal jet velocity through transient numerical simulations. However, these studies primarily focused on optimizing the air supply system, which complicates the implementation of real-time monitoring of heat losses.

Significant advancements have been made in exploring the structural design, influential factors, and testing related to air curtain airtightness. In the research of some fire and dust proof air curtain systems, the control system was mainly concerned with airflow and structure [18–21]. For example, Cheng Shen and his team [22] have proposed a novel dual Swirl Wind Curtain (DSAC) dust suppression system from the perspective of jet flow. However, the unexplored potential of data-driven deep learning intelligent algorithms for monitoring air curtain angles and airtightness remains untapped. Only in the literature [23], the feasibility of PID control of air curtain is discussed, and the calculation method of PID control parameters is defined.

Therefore, this study aims to introduce an angle control algorithm for air curtains based on a GA-optimized quadratic BP neural network (BP-GA-BP) to significantly enhance airtightness and real-time performance. The highlights of this paper include:

1. The introduction of a novel BP-GA-BP neural network algorithm addresses the limitations of current theoretical methods and simulation models by achieving the best performance of both real-time monitoring and high accuracy. It enables real-time calculation and adjustment of multiple angles with changing working conditions.
2. The proposed algorithm demonstrates improved airtightness compared to traditional control methods. The approach also requires fewer iterations, offers high computational efficiency, and achieves high fitting accuracy compared to other intelligent algorithms.
3. Utilizing the BP-GA-BP algorithms to bridge the gap in intelligent real-time control of air curtain angles enhances the accuracy of the computational model, laying the groundwork for future research in this domain.

The structure of this paper is as follows: Section 2 describes the structure and principles of the angle control system. The thorough construction of the novel BP-GA-BP algorithm is introduced in Section 3. In Section 4, the presentation of the CFD experimental procedure and airtightness indicator is provided. In Section 5, the CFD simulation results are analyzed and discussed. The paper is concluded in Section 6.

2. Architecture of the Angle Control System

Focusing on addressing the challenges related to airtightness and real-time control in air curtains, this paper introduces an angle control algorithm for air curtains utilizing a GA-optimized quadratic BP neural network. An accurate angle control model is developed utilizing a substantial amount of data from Hayes air curtain model tests [4] and

the mathematical relationship governing jet binary divergence at the windshield. In this scenario, an angle solution with high airtightness can be obtained by inputting both the internal and external temperatures measured by the sensors. The schematic of the angle control system is depicted in Figure 1.

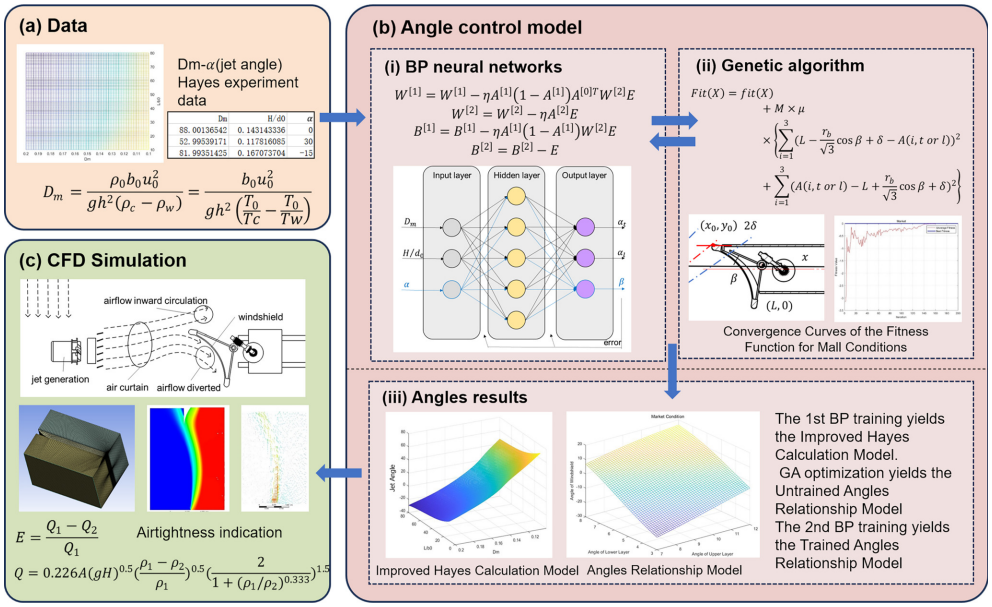


Figure 1. The architecture diagram of the angle control system.

1. Data Characterization. To achieve real-time control of the angle, a prediction model for the temperature-jet angle is initially established. The first BP neural network based on the gradient descent algorithm, designed for predicting the jet angle, is developed using Hayes air curtain model data [4].
2. Angle scheme optimization. However, traditional BP neural networks are incapable of accurately predicting the windshield angle based on the available dataset during training. To address this limitation, the study further involves the analysis and optimization modeling of the jet binary divergence problem at the windshield. The primary objective of the model is to minimize the fitness function associated with jet angles and windshield angles, aiming to closely align the performance target with the divergence target point.
3. Angle scheme training. Following the acquisition of the optimal solution set for jet angles and windshield angles through GA global search, the predictive model and optimal solution set are retrained using the BP neural network to develop the neural network model for temperature-jet angles and windshield angle.
4. Airtightness verification by CFD simulation. Moreover, the airtightness under varying control strategies and the efficacy of diverse neural network algorithms are evaluated, and the enhancement in airtightness and real-time performance is confirmed through CFD simulation.

The subsequent sections will delve deeply into the construction of the BP neural network, the analysis of the angle optimization problem, and the GA global search based on the angle control system's architecture outlined in this section.

3. BP-GA-BP Neural Network Modeling

3.1. Quadratic BP Neural Network Modeling

During the modeling process, following the initial BP neural network training, the GA-solved optimization problem of jet divergence, and the subsequent second BP neural network training, the temperature-angle model is developed, and the technology roadmap is presented in Figure 2.

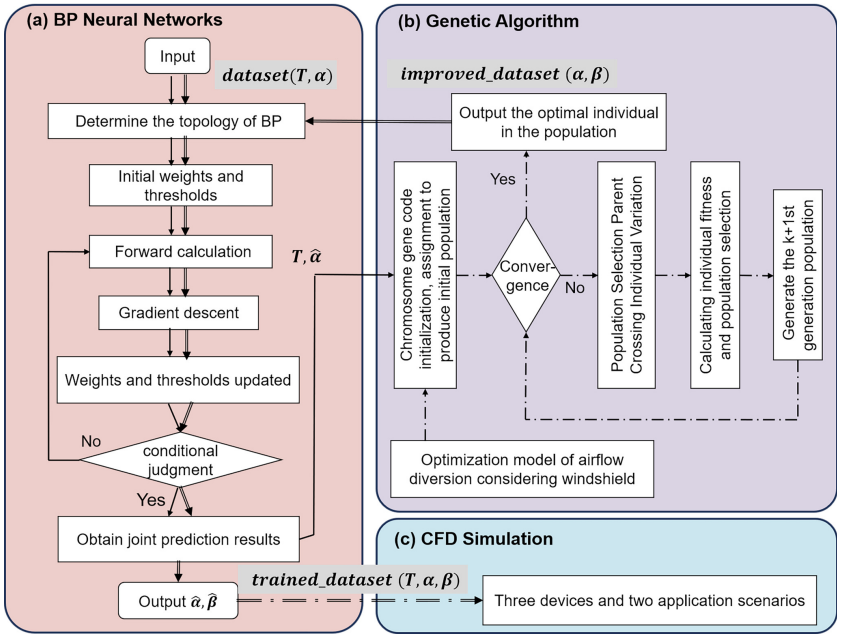


Figure 2. The technology roadmap BP-GA-BP algorithm.

A BP neural network constitutes a prevalent artificial neural network model that effectively approximates intricate, non-linear functional dependencies through its architecture, which comprises multiple layers of interconnected neurons. The back-propagation algorithm is employed to train and optimize the neural network. In this study, for the BP neural network, Hayes model dataset consists of three labels, flexural modulus D_m (see in Figure 1a), width-to-diameter ratio H/d_0 and jet deflector Angle α. D_m is determined by temperature and jet velocity. Under the condition of isothermal environment, the relationship among the three parameters is that, the air curtain jet reaches the floor.

Initially, the structure of the BP neural network consists of a single input layer, one hidden layer, and one output layer [24]. In the initial neural network configuration, there are two input nodes (D_m and H/d_0) and two output nodes (α_t and α_l) corresponding to the upper and lower jet angles. The second neural network configuration includes two input nodes representing internal and external temperatures (T_c and T_w), with the output nodes comprising α_t, α_l, and β (representing the windshield angle).

In this study, the method of optimizing the number of hidden layer neurons was adopted. The algorithm first sets an initial value and then linearly increases the number of neurons in order to find a hidden layer structure that minimizes the mean square error. During the training process, if the predicted performance is always unable to meet the requirements, consider increasing the number of hidden layers. The empirical Equation (1) for determining the number of hidden layer nodes was employed, setting an initial value of 3 as a starting point for optimization [25]. Subsequent testing revealed that when the number of hidden layer nodes n equals 5, the model's mean square error is minimized, suggesting optimal training performance, surpassing 85%.

$$n = \sqrt{n_i + n_o} + N \tag{1}$$

where, n_i denotes number of input nodes and n_o denotes number of output nodes.

Computing the error between the predicted output and the desired output, the weights and biases in the network are adjusted based on this error to enable a progressive conver-

gence of the network output towards the desired output. The Equation (2) provided outline the error function and the process for adjusting weights and biases.

$$\begin{aligned}\mathbf{W}^{[1]} &= \mathbf{W}^{[1]} - \eta\mathbf{A}^{[1]}(1-\mathbf{A}^{[1]})\mathbf{A}^{[0]T}\mathbf{W}^{[2]}\mathbf{E}\\ \mathbf{W}^{[2]} &= \mathbf{W}^{[2]} - \eta\mathbf{A}^{[2]}\mathbf{E}\\ \mathbf{B}^{[1]} &= \mathbf{B}^{[1]} - \eta\mathbf{A}^{[1]}(1-\mathbf{A}^{[1]})\mathbf{W}^{[2]}\mathbf{E}\\ \mathbf{B}^{[2]} &= \mathbf{B}^{[2]} - \mathbf{E}\end{aligned} \tag{2}$$

where, $\mathbf{W}^{[1]}$ denotes the weight of all neural nodes in the hidden layer. $\mathbf{B}^{[1]}$ denotes the threshold of all neural nodes in the hidden layer. $\mathbf{E}$ denotes the error. η denotes the learning rate. $\mathbf{A}$ denotes output of each layer.

However,the initial BP neural network faces challenges in accurately predicting the windshield angle using the current dataset. Therefore, the research delved into analyzing and resolving the jet binary divergence issue at the windshield, leveraging training from a subsequent BP neural network.

3.2. Structure and Flow Analyse

The mechanical configuration of the air curtain system primarily comprises two modules: the jet device and the arc-type windshield device, with the structural design and centerline trajectory coordinate depicted in Figure 3.

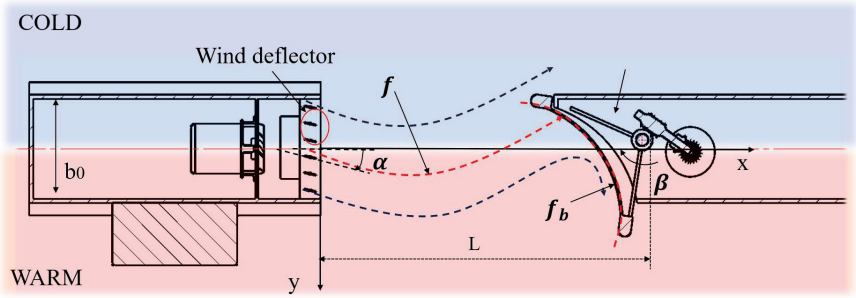


Figure 3. Air curtain mechanical structure.

Several essential components are also present, notably the fans that serve as jet generators grouped in sets of six from top to bottom. The wind deflector at the jet port is bifurcated into upper and lower parts (α_t and α_l), allowing independent adjustments upon air ejection, and ensuring comprehensive jet coverage across the air curtain doorway. A pivotal element is the rotatable curved windshield, constituting a one-sixth arc, responsible for directing jet at the closure of the air curtain boundary. The β can be adjusted as per the air curtain configuration to facilitate smooth circulation of internal and external separated jet sources.

Joao et al. [26] analyzed the momentum characteristics of the plane jet between the polluted and non-polluted regions, but did not take into account the momentum of the lateral force brought by the wind speed and pressure. But the assumption that the velocity and flow of the air on both sides are the same gave us an idea. The study of Claudio [27,28] uses the air-tightness index related to the mass transfer rate, and the mass transfer rate is related to the density, velocity, and cross-section area of the gas

Therefore, combining with the mechanical design structure in the manuscript, we set the binary divergence of the jet at the windshield as the optimization target of the genetic algorithm. In more detail, we express the central track line of the jet so that it intersects with the windshield, as depicted in Figure 3.

3.3. Optimization Problem Modeling

Optimization problems represent a subset within the domain of mathematical problems that necessitate the identification of optimal values for variables, the evaluation of

an objective function, and the satisfaction of constraints. The manipulation of these optimization variables is central to the process of minimizing or maximizing the objective function's value. This section is dedicated to the development of optimization models pertaining to air curtain configurations, and the application of the genetic algorithm for their resolution, considering the absence of windshield angles β in the Hayes dataset and the mathematical relationship between angles.

In stable working conditions, the indoor environment remains practically isothermal and the air jet is roughly at the nominal indoor temperature T_c. As metioned above, the chromosome can be expressed as the Equation (3):

$$X = \{\alpha_t, \alpha_l, \beta\} \tag{3}$$

Six jet velocities and two jet angles yield six center trajectory lines, and the equation is given in Equation (4) [29].

$$f : y = -\frac{C_n T_c w^2}{8 T_w u^2 b_0 \cos\alpha} x^2 + x \tan\alpha \tag{4}$$

where, w is the outside wind speed, generally taking 3.5 m/s; C_n is the constant coefficient, taking 0.5.

The expression of the windshield curve is shown in Equation (5):

$$f_b : (x - (L - \frac{2r_b}{\sqrt{3}} \cos(\beta + \frac{\pi}{3})))^2 + (y - \frac{2r_b}{\sqrt{3}} \sin(\beta + \frac{\pi}{3}))^2 = {r_b}^2 \tag{5}$$

where, L is the width of door. r_b is the radius of the windshield arc. β is the anlge of windshield.

The point on the windscreen curve f_b closest to the Y-axis is defined as the reference target point(RTP), which is expressed as:$(x_0, y_0) = (L - \frac{r_b}{\sqrt{3}} \cos\beta, \frac{r_b}{\sqrt{3}} \sin\beta)$. The intersection of the windshield curve and the center trajectory lines is defined as the actual target point(ATP). Theoretically, when the ATP coincides with the RTP, our optimization goal: binary divergence at the windshield can be achieved. However, there are chances for ATP of falling in the side region. Thus, to prevent instances of such a problem, as well as to conserve computational resources and time, a virtual straight line segment parallel to the X-axis is established, as depicted in Figure 4. This line segment, with (x_0, y_0) at its midpoint, is expressed as Equation (6)

$$l_0 : x \in (x_0 - \delta, x_0 + \delta), y = y_0 \tag{6}$$

where, δ is half of the length of the virtual straight line segment.

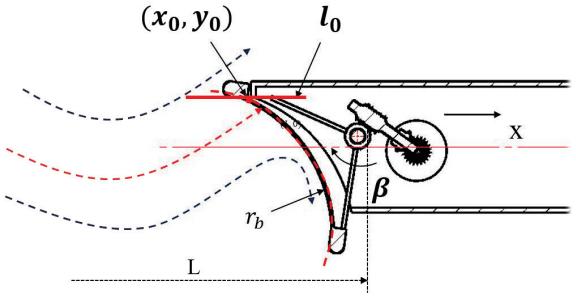


Figure 4. Binary divergence of the flow.

If the center line trajectory equation has no intersection with the virtual straight line segment, the angles α_t, α_l and β need to be recalculated and calibrated. The proximity to the target point could only be calculated when there exists an intersection point. In summary, the constraints consist of inequality and equation conditions are obtained to

define the feasible solution space of the problem.The objective function is defined as a measure of the overall proximity of the six ATPs to the RTP in the X -axis direction, as shown in Equation (7).

$$\min : \left\{ \sum_{i=1}^{k} x_i - k \times \left(L - \frac{2r_b}{\sqrt{3}} \cos(\beta + \frac{\pi}{3}) \right) \right\}^2 \tag{7}$$

where, k is the number of ATP.

The fitness of an individual refers to the measure of the degree of superiority of an individual in the survival of a population, which is calculated using the fitness function. Then, the equation constraints are brought into the objective function so that the objective function is transformed into a fitness function (8) containing only the input variables X.

$$\begin{aligned} fit(X) = &- \{A(1,t) + A(2,t) + A(3,t) \\ &+ A(4,l) + A(5,l) + A(6,l) \\ &- 6 \times (L - \frac{r_b}{\sqrt{3}} \cos\beta)\}^2 \end{aligned} \tag{8}$$

where, for ease of presentation, $A(i,t)$ is a shorthand for the following Equation (9), and $A(i,l)$ is the same.

$$A(i,t) = \frac{\tan\alpha_t + \sqrt{\tan\alpha_t{}^2 - \frac{C_n T_c w^2 r_b \sin\beta}{2T_w u_i{}^2 \sqrt{3} b_0 \cos\alpha_t}}}{\frac{C_n T_c w^2}{4T_w u_i{}^2 b_0 \cos\alpha_t}} \tag{9}$$

The optimization problem studied in this paper incorporated inequality constraints, necessitating the use of a penalty function approach to address them. By transforming these constraints into a properly defined composite function and incorporating it into the original objective function, a new fitness function (10) is derived.

$$\begin{aligned} Fit(X) = &fit(X) + M \times m \\ &\times \{ \sum_{i=1}^{3} (L - \frac{r_b}{\sqrt{3}} \cos\beta + \delta - A(i, torl))^2 \\ &+ \sum_{i=1}^{3} (A(i, torl) - L + \frac{r_b}{\sqrt{3}} \cos\beta + \delta)^2 \} \end{aligned} \tag{10}$$

where, M is initial penalization factor. m is external electric penalty function, the iteration point is then outside the feasible domain for the inequality constraints to work [30].

The genetic algorithm is a guided stochastic search method designed for solving optimization problems with robust global search and optimization capabilities. The program initiates with a population individuals undergoing iterations. During the crossover operation and mutation operation, two individuals exchange parts of their genetic material or random changes happen in an individual's gene composition.

Thus, the overall training architecture is presented in Figure 5. The blue bullet in the figure highlight the output of the newly added windshield Angle β during the second neural network training process.

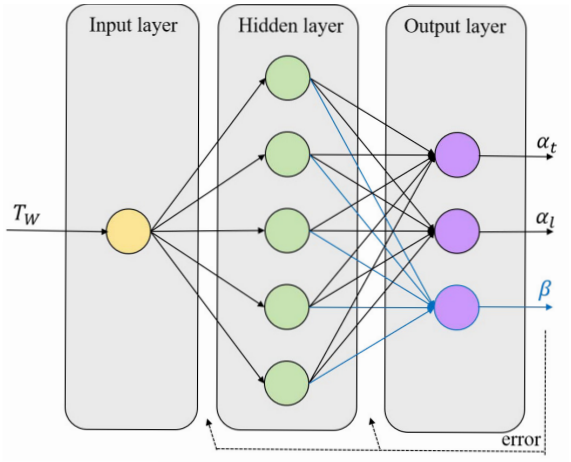


Figure 5. BP-GA-BP architecture.

4. CFD Simulation Procedure

4.1. Airtightness Indication

When assessing the effectiveness of an air curtain, various key performance indicators, such as service life, isolation capabilities, energy efficiency, noise levels, among others, must be taken into account to guarantee that its practical implementation can deliver the desired outcomes.

The pioneering empirical equation for the infiltration rate algorithm was introduced by Brown and Solvason [31]. Subsequently, many researchers [32–35] refined the coefficients. Finally, the refined Equation (11) is presented as follows.

$$Q = 0.226A(gH)^{0.5}\left(\frac{\rho_1 - \rho_2}{\rho_1}\right)^{0.5}\left(\frac{2}{1 + \left(\frac{\rho_1}{\rho_2}\right)^{0.333}}\right)^{1.5} \tag{11}$$

where, A is the area of the door with the air curtain installed. ρ_1 and ρ_2 are the average densities of the inside and outside air in kg/m^3, respectively.

Gonçalves et al. [10] computed the sealing efficiency of air curtains using two distinct methods based on the mass and heat of the air entering the freezer, respectively. To ensure consistency in metric measurements under isothermal and non-isothermal environmental, the air infiltration rate is employed as a benchmark for evaluating air curtain performance in terms of efficiency metrics [9]. The equation for efficiency calculation (12) is provided as follows.

$$E = \frac{Q_1 - Q_2}{Q_1} \tag{12}$$

where, E is the airtightness of the air curtain. Q_1 is space air infiltration rate without air curtain installation. Q_2 is space air infiltration rate after installation of air curtain.

4.2. Simulation

The BP-GA-BP neural network algorithm will be implemented on the CFD model by ANSYS Fluent software (ANSYS 2022 R1). Its creator is ANSYS, Inc. in Canonsburg, Pennsylvania, United States. With the help of CFD, it is simple and low-cost numerically solve the differential equations controlling fluid flow to obtain a discrete distribution of the flow field over a continuous region of the fluid flow, which provides an approximation of the actual fluid flow situation.

During the meshing phase preceding the simulation, local mesh refinement was conducted on the nozzle of the air curtain device under investigation. Consequently, the mesh was divided into a refined section of 5 mm and a coarser section of 20 mm, enabling a more detailed recording of the jet dynamics near the inlet. The simulation duration was set at 30 s, and a mesh size of 1 mm was selected. The k-epsilon model was used to simulate

fluid viscosity behavior, and the energy field simulation was activated. Furthermore, the air model was defined as a real gas with a gravitational acceleration of 9.8 m/s^2 considered. The indoor Y-direction boundaries and the air curtain windbreak positions were treated as wall boundary conditions to emulate realistic wall effects. The outdoor X-direction planes and the middle area of the air curtain opposite to the Z-direction were designated as velocity_inlet boundary conditions, while the velocity inlet opposite to the Z-direction was positioned based on various simulation predictions. The remaining planes were then defined as pressure-out boundary conditions to simulate external ambient pressure.

The study outlines two application scenarios based on the operational conditions of a cold storage and a shopping mall. These scenarios share the same environmental parameters, including the height (2000 mm) and width (3000 mm) of the door, the width of the air curtain (200 mm), and wind speed (3.5 m/s), but differ in temperature.The temperature of the cold storage, T_c, is 255.15 Kelvin, and the temperature of the warm storage, T_w, is 293.15 Kelvin. The temperature of the shopping mall, T_c, is 298.15 Kelvin, and the temperature of the warm storage, T_w, is 313.15 Kelvin.

5. Verification and Discussion

5.1. Airtightness Verification

5.1.1. Proposed BP-GA-BP Algorithm

Simulation verification is carried out based on the angle control system proposed in this paper to characterize the thermal insulation effect of the air curtain in terms of airtightness. In the two conditions, simulations are conducted for three groups of control schemes at four key time nodes: the initiation state (t = 0.5 s), the unsteady states (t = 1.0 s and t = 1.5 s), and the steady state (t = 5.0 s). The simulation effect diagrams for these conditions are depicted in Figure 6.

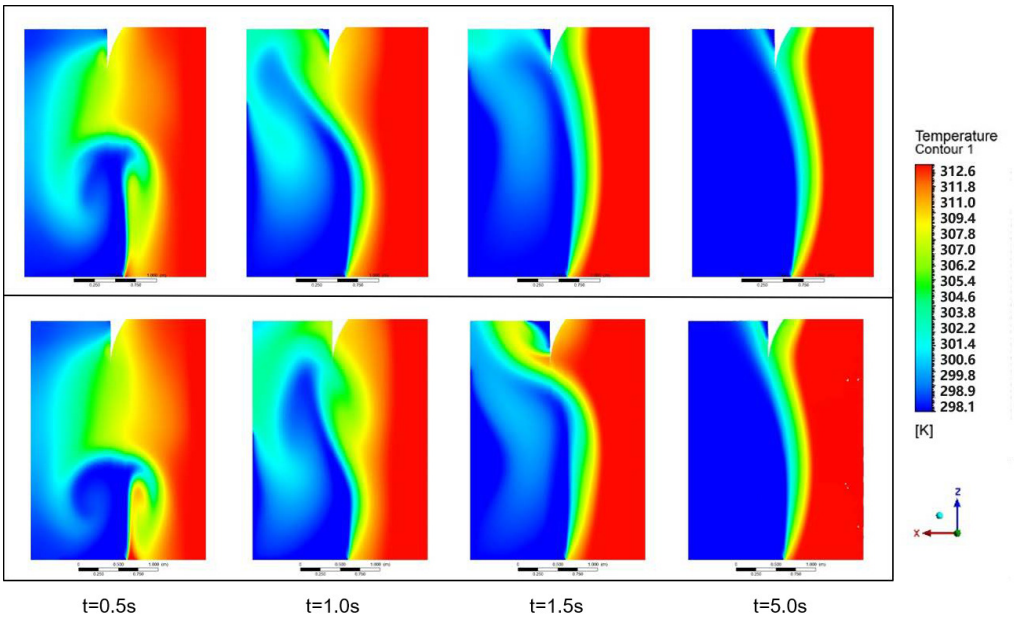


Figure 6. Simulation effect diagram.

The simulation results, along with the analysis of the air curtain efficiency data presented in Table 1, indicate that the BP-GA-BP algorithm's control scheme effectively captures the jet device's incidence angle, ensuring that the wind baffle directs a portion of the outflowing wind away from the interior. Consequently, the occurrence of tail deflection is significantly mitigated. The calculated airtightness values, by Equation (12), are 86% and 82% for the respective cases. Thus, it is demonstrated that the angle control scheme proposed in this study exhibits enhanced airtightness performance.

Table 1. Airtightness calculation value for simulation.

Condition	Airtightness (%)			Improvement (%)
	CONTROL X	CONTROL Y	CONTROL Z	Z vs. Y
Cold storage	0	68	86	26.5
Shopping mall	0	57	82	43.9

5.1.2. Comparison with Other Control Schemes

This study also evaluates the airtightness of the proposed algorithm in contrast to conventional control strategies. The simulation outcomes for three distinct control schemes are illustrated in Figure 7. These include CONTROL X, which models natural convection conditions; CONTROL Y, a conventional algorithm with a selected jet angle α of 5°; and CONTROL Z, which employs the BP-GA-BP algorithm developed in this research.

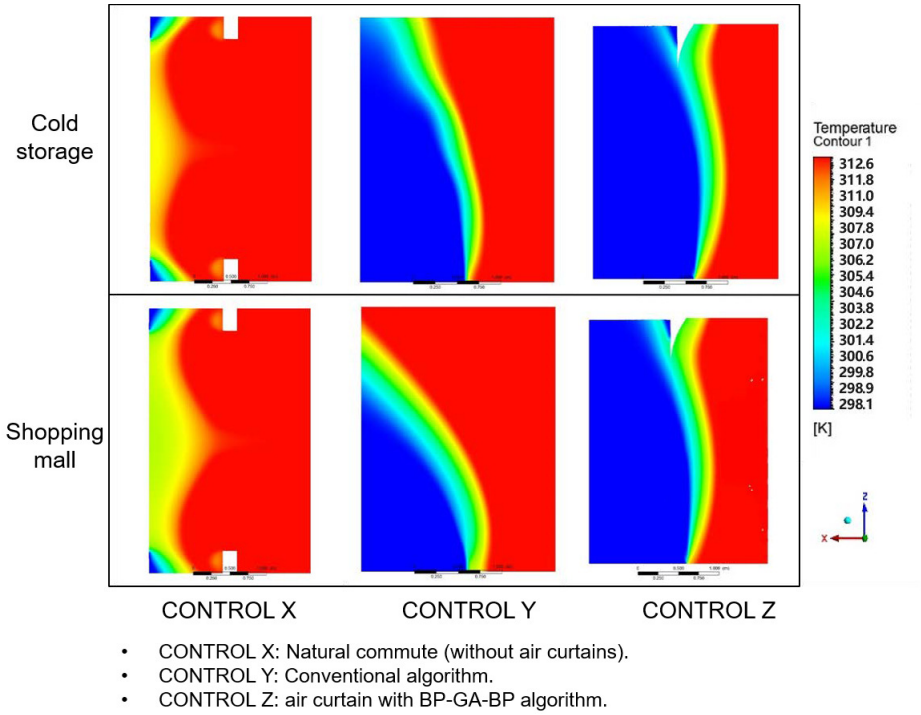


Figure 7. Simulation outcomes for three distinct control schemes.

Observation can be made regarding the thermal behavior of different controls. Initially, heat transfer through natural convection started at 0.5 s at both the hot and cold temperature junctions at the gate entrance. Subsequently, in CONTROL X, thermal jet continued to enter the gate at 1 s and 1.5 s, with certain sections approaching a steady state by 3 s. Additionally, in CONTROL Y, thermal jet reached the distal end at 1 s and 1.5 s, causing a deflection in the jet field direction. There was a marked reduction in jet velocity for the air curtain, with the doorway nearing a steady state by 5 s. In contrast to CONTROL Z, a pronounced deflection of the tail occurred at this point.

The airtightness of CONTROL Y was measured as 68% under cold storage conditions and 57% in mall conditions. Consequently, the efficiencies of the air curtains improved by 26.5% and 43.9%, as indicated in Table 1. Therefore, it can be inferred that the intelligent control scheme proposed in this study surpasses conventional methods in enhancing air curtain efficiency.

5.1.3. Comparison with Experimental Results

On the basis of the previous simulation analysis, further experiments are conducted to verify the proposed control scheme of improving the airtightness. The size parameters and

temperature settings of the experimental device is consistent with the simulation model. In order to ensure a better resultsncomparison between the experimental and the simulation, two periods of time when the average ambient temperature outside the library was close to 293.15 Kelvin and 313.15 Kelvin were selected for startup test during the test. After the air curtain device runs stably, the average temperature was measured and compared with the set temperature. The experiment was repeated three times, and the results of each group were shown in the Table 2.

Table 2. Airtightness calculation value for experiment.

Condition	Airtightness (%)			Improvement (%)
	CONTROL X	CONTROL Y	CONTROL Z	Z vs. Y
Cold storage	0	63.6	80.3	26.3
Shopping mall	0	51.2	72.4	41.4

The experimental results show that the proposed control scheme can effectively improve the air tightness compared with the traditional control scheme, which is consistent with the simulation results and conclusions. Comparing the air-tightness results of simulation and experiment, it is found that the former is always slightly higher than the latter. This may be attributed to the parameter measurement error of the experimental device, and the control error makes the air tightness deviation. And the effect of actual conditions on air flow and temperature is not taken into account. Based on the above factors, the conclusion of consistency between simulation model and experiment can still be drawn.

5.2. Algorithm Performance Verification

5.2.1. Proposed BP-GA-BP Algorithm

To verify the accuracy and effectiveness of our proposed BP-GA-BP neural network model, test data from a structural air curtain is collected as an example for experimental evaluation. Based on the theoretical calculation model proposed by Hayes [4] and the windscreen optimization model mentioned above, the test data set is obtained, and its size is 1125, which is determined by the temperature difference between inside and outside and the step size. Each test data point contains one input variable (T1, T2) and three output variables (a1,a2,b). 80% of these points are used for training, while 20% are reserved for testing. As mentioned above, a three-layer neural network with a structure of 1-5-3 is used in this experiment, with a maximum number of iterations set to 1000 and an objective error target of 0.001. The genetic algorithm program begins with a population of 60 individuals and runs for 200 iterations. In crossover, there is an 80% chance that two individuals will exchange some of their genes, while in mutation, there is a 10% chance that a gene will be randomly altered. Epochs, Mean Squared Error (MSE), Root Mean Squared Error (RMSE), R-squared (R2), and Mean Absolute Error (MAE) are chosen as our evaluation metrics to evaluate the performance of the neural network.

The prediction results and performance of the BP-GA-BP algorithm are visualized in Figures 8 and 9, illustrating good convergence and robustness. Analysis of the training performance graphs for the BP neural network indicates that the algorithm efficiently fits data from the training, validation, and test sets, owing to its gradual convergence and strong generalization capabilities throughout the training process. Additionally, the GA demonstrates robust convergence with the fitness function across iterations, with no abnormalities observed in the crossover and mutation processes.

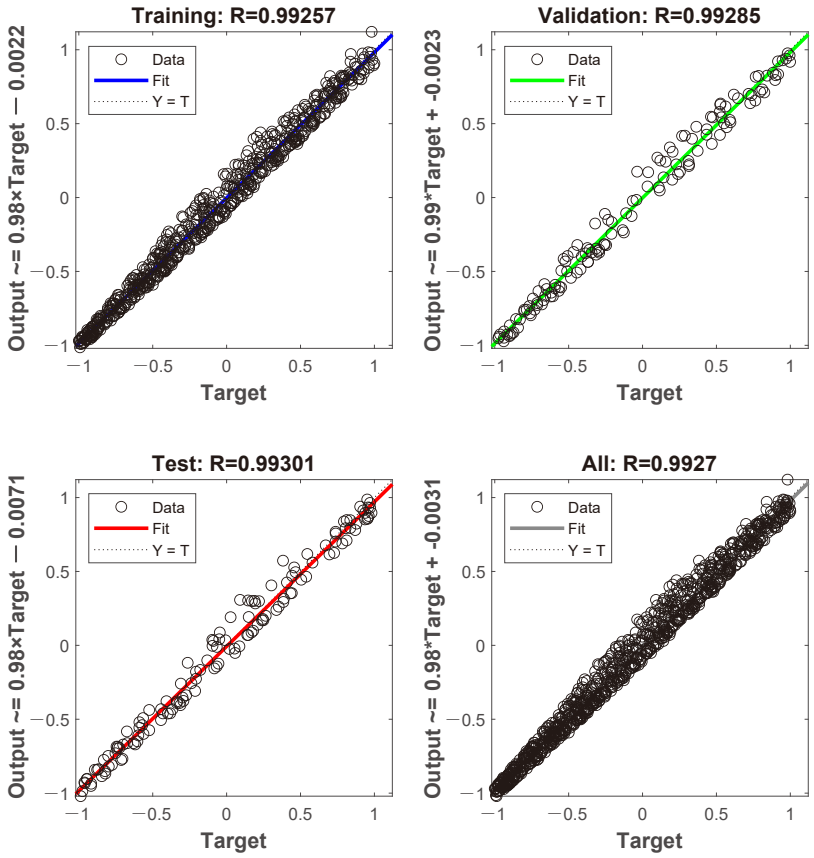


Figure 8. Lgorithm goodness of fit: R-squared.

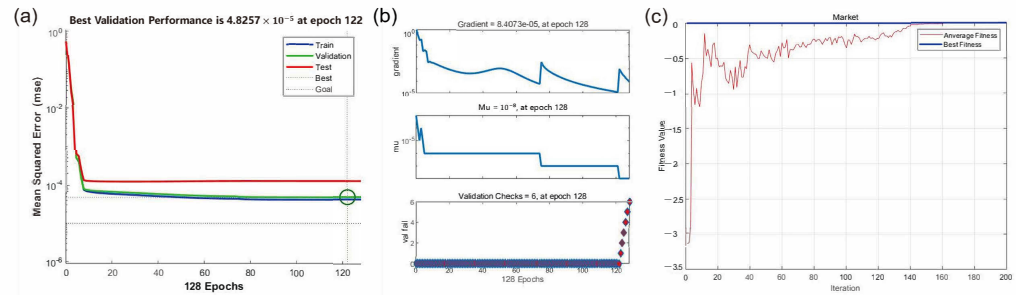


Figure 9. (**a**) lNumber of evolutionary generations. (**b**) Algorithm performance. (**c**) Training state.

5.2.2. Comparison with Other Algorithms

In this study, real-time performance refers to the computational efficiency of updating the model when factors such as external pressure and jet velocity change. Due to the lack of research on air curtain intelligent control, the proposed algorithm is horizontally compared with other BP neural network algorithms. The experiments in this study are categorized into four groups (labeled as No. 1–No. 4) based on the data feature processing for the first BP neural network and angle scheme optimization for GA algorithms. Performance metrics are compared by conducting neural network model training, and the outcomes of the comparison are presented in Table 3.

The comparison results demonstrate that the BP-GA-BP neural network algorithm outperforms other BP neural network algorithms across all performance metrics. Compared to the standard BP neural network (No. 1), the BP-GA-BP algorithm reduced the number of epochs by 89%, and it notably decreased MSE, RMSE and MAE by 97.8%, 86.4%, and 85.2%,

respectively. Similar to the findings of previous studies, the R2 values were slightly improved, although not significantly, and all the BP algorithms exhibited superior goodness of fit. The use of BP neural networks for data feature processing (No. 2) significantly enhanced the performance metrics of MSE, RMSE, and MAE, leading to a substantial improvement in computational accuracy compared to traditional fitting methods, Polynomial Curve Fitting. Concurrently, the genetic algorithm was employed to optimize the perspective scheme of the BP neural network model, thereby preventing convergence to local optima. Analysis of the experimental results after incorporating the genetic algorithm (No. 3) for optimization revealed a substantial reduction in the number of epochs, suggesting a marked improvement in computational efficiency and a minor enhancement in computational accuracy. In conclusion, the BP-GA-BP neural network algorithm presented in this study exhibits advantages over other BP neural network algorithms in terms of reduced iterations and enhanced real-time performance.

Table 3. Comparison results with other algorithms.

No.	Algorithm	Epoch	MSE	MAE	RMSE	R^2
1	Polynomial Curve Fitting + Newton's method + BP	879	0.119900	0.09122	0.109541	0.9927
2	BP+Newton's method + BP	864	0.070589	0.06951	0.084088	**0.9987**
3	Polynomial Curve Fitting(PCF) + GA + BP	256	0.004161	0.01404	0.020397	0.9959
4	BP + GA + BP	122	**0.002691**	**0.01239**	**0.016097**	**0.9987**

The bolded numbers highlight the maximum value of the indicator.

Further, algorithms No. 3 and No. 4 are selected and their parameter robustness is compared and analyzed. These factors, the number of samples, the number of hidden layers and the number of nodes, can directly or indirectly affect the performance of neural network algorithms [36]. The results of the algorithm are shown in Table 4.

Here, the number of samples is selected as a factor to explore its influence on the algorithm running time and R-square value. When the number of training samples increases from 50 to 3000, the running time of algorithm No.4 (BP + GA + BP) changes within 1s. However, algorithm No.3 (PCF + GA + BP) takes longer running time and increases significantly with the increase of sample size. For R-square values, both algorithms have a significant improvement, reaching their maximum values at 1500 and 2000, respectively. Therefore, the algorithm proposed in this paper is more robust.

Table 4. Number of samples results.

Number of Samples	PCF + GA + BP		BP + GA + BP	
	Time (s)	R^2	Time (s)	R^2
50	4.7877	0.9578	8.5258	0.8432
100	4.855	0.9740	9.1545	0.8661
500	4.9448	0.9831	11.6454	0.9234
1000	4.9672	0.9928	12.4534	0.9464
1500	5.0352	0.9970	13.0576	0.9831
2000	5.3171	0.9929	13.5678	0.9959
3000	5.2788	0.9928	13.5678	0.9942

6. Conclusions

This paper proposes an angle control algorithm for air curtains, which is based on a GA-optimized quadratic BP neural network and aims to enhance airtightness and enable real-time control. Initially, a BP neural network based on gradient descent is developed for predicting the injection angle. Subsequently, the issue of minimizing the jet divergence

at the windshield is modeled, and an optimization model is established to fulfill the performance requirements. Additionally, GA's global search capabilities are employed to identify the optimal solution set for the jet angle-windshield angle, followed by the training of the BP neural network to yield the final angles control model. Furthermore, the benefits of the proposed control scheme, including improved airtightness and real-time performance, are confirmed through CFD simulations. The primary contributions of this study encompass:

1. The introduction of an innovative BP-GA-BP neural network algorithm, which exhibits enhanced airtightness, surpassing both conventional control strategies and existing intelligent algorithms. The proposed algorithm yielded 26.5% and 43.9% improvements under two distinct operational scenarios.
2. Resolution of limitations in existing theoretical methodologies and simulation models for air curtains, enabling real-time monitoring and more precise adjustments in multiple angle calculations. The BP-GA-BP algorithm, in comparison to the conventional approach, achieved an 89% reduction in Epoch, and significant decreases in MSE, RMSE, and MAE by 97.8%, 86.4%, and 85.2%, respectively, as well as a stronger robustness.
3. The application of artificial intelligence algorithms bridges the gap in intelligent real-time control of air curtain angles, offering a novel approach to advancing air curtain technology and contributing to energy conservation and emission reduction. This study sets the stage for future research in the field.

Based on the mechanical design structure of the air curtain proposed in this paper, the intelligent control of the air curtain is realized by using neural network algorithm. It is innovative in its algorithm and structure. Theoretically, the algorithm is suitable for air curtains with different structural parameters. For air curtains of other structures, such as circulating air curtains and non-circulating air curtains, they cannot be directly applied due to different airflow characteristics and structures. However, the algorithm architecture proposed in this paper can provide ideas and references for other structural air curtains. In the future, the team will also continue relevant research in the two aspects of structural design and algorithm universality.

Author Contributions: Conceptualization, methodology, software, verification, formal analysis, and manuscript writing were implemented by Y.Z. (Yuxi Zhao). Conceptualization, resources, and review and editing were carried out by L.S. and H.Z. Investigation and data collation were realized by Y.Z. (Yuhang Zheng). All authors have read and agreed to the published version of the manuscript.

Funding: This research was funded by NSFC, grant number 62476057.

Data Availability Statement: Data are contained within the article.

Conflicts of Interest: The authors declare no conflicts of interest.The funders had no role in the design of the study; in the collection, analyses, or interpretation of data; in the writing of the manuscript; or in the decision to publish the results.

References

1. Downing, C.C.; Meffert, A.W. Effectiveness of cold-storage door infiltration protective devices. *Ashrae Trans. Am. Soc. Heat. Refrig.-Air-Cond. Eng.* **1993**, *99 Pt 2*, 356–366.
2. Azzouz, A.; Gosse, J.; Duminil, M. Experimental determination of cold loss caused by opening industrial cold-room doors. *Int. J. Refrig.* **1993**, *16*, 57–66 [CrossRef]
3. Gil-Lopez, T.; Castejon-Navas, J.; Galvez-Huerta, M.A.; O'Donohoe, P.G. Energetic, environmental and economic analysis of climatic separation by means of air curtains in cold storage rooms. *Energy Build.* **2014**, *74*, 8–16. [CrossRef]
4. Hayes, F.C.; Stocker, S.W. Heat transfer characteristics of air curtain. *Ashrae Trans. Ons* **1969**, *1*, 167–179
5. Jerning, G.E. Air curtain in the 70's. *Refrig. Air Cond.* **1970**, *3*, 93–99
6. Sadowski; Mirosław; Kuriata, A.; Jelonek, B. Przestepstwo Pospolite Czy Podatkowe? Zbieg Czynów Zabronionych w Rozumieniu art. 8 s 1 k.k.s. w Swietle Najnowszego Orzecznictwa Sadu Najwyzszego. 2011. Available online: http://www.repozytorium.uni.wroc.pl/dlibra/publication/edition/65430 (accessed on 20 June 2024).
7. Guyonnaud, L.; Solliec, C.; DeVirel, M.D.; Rey, C. Design of air curtains used for area confinement in tunnels. *Exp. Fluids* **2000**, *28*, 377–384. [CrossRef]

8. Foster, A.M.; Swain, M.J.; Barrett, R.; D'Agaro, P.; Ketteringham, L.P.; James, S.J. Three-dimensional effects of an air curtain used to restrict cold room infiltration. *Appl. Math. Model.* **2007**, *31*, 1109–1123. [CrossRef]
9. Foster, A.M.; Swain, M.J.; Barrett, R.; D'Agaro, P.; James, S.J. Effectiveness and optimum jet velocity for a plane jet air curtain used to restrict cold room infiltration. *Int. J. Refrig.* **2006**, *29*, 692–699. [CrossRef]
10. Gonçalves, J.C.; Costa, J.J.; Lopes, A.M.G. Parametric study on the performance of an air curtain based on CFD simulations—New proposal for automatic operation. *J. Wind. Eng. Ind. Aerodyn.* **2019**, *193*, 103951. [CrossRef]
11. Gonçalves, J.C.; Costa, J.J.; Figueiredo, A.R.; Lopes, A.M. CFD modelling of aerodynamic sealing by vertical and horizontal air curtains. *Energy Build.* **2012**, *52*, 153–160. [CrossRef]
12. Gonçalves, J.C.; Costa, J.J.; Figueiredo, A.R.; Lopes, A.M.G. Study of the aerodynamic sealing of a cold store—Experimental and numerical approaches. *Energy Build.* **2012**, *55*, 779–789. [CrossRef]
13. Rai, A.; Sun, J.; Tassou, S.A. Three-dimensional investigation on the positioning of air curtain on its effectiveness in refrigerated vehicles used for food distribution. *Energy Procedia* **2019**, *161*, 224–231. [CrossRef]
14. Rai, A.; Sun, J.; Tassou, S.A. Numerical investigation of the protective mechanisms of air curtain in a refrigerated truck during door openings. *Energy Procedia* **2019**, *161*, 216–223. [CrossRef]
15. Rai, A.; Sun, J.; Tassou, S.A. Numerical investigation into the influence of air curtain discharge angles in refrigerated trucks. *Energy Procedia* **2019**, *161*, 207–215. [CrossRef]
16. Sun, J.; Tsamos, K.M.; Tassou, S.A. CFD comparisons of open-type refrigerated display cabinets with/without air guiding strips. *Energy Procedia* **2017**, *123*, 54–61. [CrossRef]
17. Sihwan, L. Study on Energy Loss in Open-Gate Cooling (Part 1) Numerical Study on Ventilation Volume and Air Curtain Thermal Interception Characteristics in a Single Opening. 2018. Available online: https://jglobal.jst.go.jp/detail?JGLOBAL_ID=201802235597982264 (accessed on 22 June 2024).
18. Li, X.; Zhang, M.; Jiang, Y.; Wang, L.; Zhao, X.; Chang, X.; Bai, H.; Deng, X. Air Curtain Dust-Collecting Technology: Investigation of Factors Affecting Dust Control Performance of Air Curtains in the Developed Transshipment System for Soybean Clearance Based on Numerical Simulation. *Powder Technol.* **2022**, *396*, 59–67.
19. Xiu, Z.; Nie, W.; Cai, P.; Chen, D.; Zhang, X. Partially Enclosed Air Curtain Dust Control Technology to Prevent Pollution in a Fully Mechanized Mining Face. *J. Environ. Chem. Eng.* **2022**, *10*, 108326. [CrossRef]
20. Nie, W.; Zhang, Y.; Guo, L.; Zhang, X.; Peng, H.; Chen, D. Research on Airborne Air Curtain Dust Control Technology and Air Volume Optimization. *Process. Saf. Environ. Prot.* **2023**, *172*, 113–123. [CrossRef]
21. Wang, J.; Du, C.; Du, S.; Jin, W.; Fan, D. Dust Dispersion Law and High-Pressure Air Curtain Control Technology of Crossheading during the Process of Ore Unloading. *J. Wind. Eng. Ind. Aerodyn.* **2022**, *230*, 105179. [CrossRef]
22. Shen, C.; Wang, D.; Zhang, J.; Bi, Q. A Novel Dual Swirling Air Curtain Dust-Control System: Design and Similar Experiment. *J. Environ. Chem. Eng.* **2024**, *12*, 113728. [CrossRef]
23. Yu, L.; Chen, Y.; Chen, S.; Zhang, Y.; Zhang, H.; Liu, C. Numerical Analysis of the Performance of a PID-Controlled Air Curtain for Fire-Induced Smoke Confinement in a Tunnel Configuration. *Fire Saf. J.* **2023**, *141*, 103930. [CrossRef]
24. Zhang, J.; Zhao, X.; Gao, Y. Shear strength prediction and failure mode identification of beam–column joints using bpnn, rbfnn, and grnn. *Arab. J. Sci. Eng.* **2023**, *48*, 4421–4437. [CrossRef]
25. Li, Y.Y.; Zhang, F.; Su, J. Improvement of the bayesian neural network to study the photoneutron yield cross sections. *Nucl. Sci. Tech.* **2022**, *33*, 135. [CrossRef]
26. Viegas, J.C.; Oliveira, F.; Aelenei, D. Experimental Study on the Aerodynamic Sealing of Air Curtains. *Fluids* **2018**, *3*, 49. [CrossRef]
27. Claudio, A.R.; van Hooff, T.; Blocken, B.; van Heijst, G. Air Curtain Performance: Introducing the Adapted Separation Efficiency. *Build. Environ.* **2021**, *188*, 107468.
28. Ruiz, C.A.; van Hooff, T.; Blocken, B.; van Heijst, G. Restriction of Air Infiltration by an Air Curtain Optimized with Secondary Jets—A Numerical Investigation. In Proceedings of the ASHRAE Topical Conference Proceedings, Denver, CO, USA, 10–12 November 2021; Indoor Air Quality.
29. Tang, X.L.; Shi, Z.Z. Theoretical study on sealing characteristics of gas curtain under lateral flow. *Build. Heat Vent. Air Cond.* **1999**, *2*, 6–8.
30. Sahoo, L.; Mahato, S.K.; Bhunia, A.K. Optimization of system reliability in the imprecise environment via genetic algorithm. *Int. J. Swarm Intell. Res.* **2022**, *13*, 1–21. [CrossRef]
31. Brown, W.G.; Solvason, K.R. Natural convection through rectangular openings in partitions—1: Vertical partitions. *Int. J. Heat Mass Transf.* **1962**, *5*, 859–868. [CrossRef]
32. Tamm, W. Kalterveluste durch kuhlraumoffnungen. *Kaltetechnik-Klimatisierung* **1966**, *18*, 142–144
33. Fritzsche, C.; Lilienblum, W. Neue messengun zur bestimmung der kalterluste an kuhlraumturen. *Kaltetechnik-Klimatisierung* **1968**, *20*, 279–286.
34. Gosney, W.B.; Olama, H.; Levy, F. Heat And Enthalpy Gains Through Cold Room Doorways. *Inst. Refrig. Proc.* **1976**, *72*, 31–41. Available online: http://pascal-francis.inist.fr/vibad/index.php?action=getRecordDetail&idt=PASCAL7870469733 (accessed on 27 September 2024).

35. Pham, Q.T.D.; Oliver, W. Infiltration of Air into Cold Stores. Meat Institute of New Zealand 16th Internat 1983, Volume 6. Available online: https://www.aivc.org/resource/infiltration-air-cold-stores#:~:text=Measures%20air%20exchange%20across%20open%20cold%20store%20doors%20using%20an (accessed on 27 September 2024).
36. Zhang, H.; Cheng, J.; Zhang, J.; Liu, H.; Wei, Z. A Regularization Perspective Based Theoretical Analysis for Adversarial Robustness of Deep Spiking Neural Networks. *Neural Netw.* **2023**, *165*, 164–174. [CrossRef]

Disclaimer/Publisher's Note: The statements, opinions and data contained in all publications are solely those of the individual author(s) and contributor(s) and not of MDPI and/or the editor(s). MDPI and/or the editor(s) disclaim responsibility for any injury to people or property resulting from any ideas, methods, instructions or products referred to in the content.